Simulations of Turbulent Drag Reduction Using Micro-Bubbles

M.R. Maxey, J. Xu, S. Dong and G. E. Karniadakis
Center for Fluid Mechanics, Turbulence and Computation
Division of Applied Mathematics, Brown University
Providence, RI 02912 USA

A series of numerical simulations of turbulent channel flow have been made to investigate the dynamical effects of seeding the flow with micro-bubbles up to average void fractions of 10%. Initial near-wall seeding in general leads to a transient reduction in drag while seeding with smaller bubbles is more effective in producing sustained drag reduction.

1. INTRODUCTION

McCormick & Bhattacharyya [1] first demonstrated that the presence of gas micro-bubbles in water in a turbulent boundary layer flow can produce a significant reduction in the drag at the wall. This feature has been verified in a series of experimental studies by Madavan et al. [2,3]; see also the review article of Merkle & Deutsch [4]. Air or gas injected through a porous plate mounted in the boundary layer forms small bubbles that are observed to lead to reductions of 20-30%, and higher, in the wall shear stress, depending on the rate of gas injection. Experiments have been reported more recently by Kato et al. [5], Guin et al. [6] and Kato et al. [7], and in the past proceedings of this symposium [8]. Detailed measurements have proved to be very difficult and there are still many open questions about the dynamics involved.

Recently we reported on simulations of a turbulent channel flow seeded with spherical micro-bubbles in which it was shown that drag could be reduced by 10%, see Xu et al. [9]. These flows were seeded with up to 800 bubbles. Both bubble size and near-wall concentration were found to be important factors with the smallest bubbles giving a sustained level of drag reduction. Kanai &Miyata [10] performed simulations for a turbulent channel flow seeded with 27 bubbles and Kawamura & Kodama [11] used a front-tracking scheme to compute the flow with up to 54 bubbles. These results at present are inconclusive as to drag reduction and in general they have considered larger bubbles dispersed throughout the flow. Here we present results involving a range of bubble sizes, seeding levels and flow Reynolds numbers.

Many factors may contribute to the drag reduction mechanism including bubble deformation or evolution of the bubble sizes by splitting or coalescence. Here we focus on a narrower set of issues. The bubbles are assumed to remain nearly spherical under the action of surface tension. This is appropriate for small micro-bubbles for which the Weber number is small. Surface contamination of the micro-bubbles, especially in seawater, will lead to an approximately rigid, no-slip surface as described in Magnaudet & Eames [12] and Detsch [13]. While these are major simplifications the results obtained point to the dynamical effects that are represented in the simulations and play a role in the reduction in drag.

2. EQUATIONS OF MOTION

The coupled two-phase flow dynamics of the micro-bubbles and the turbulence is represented by the force-coupling method (FCM) introduced by Maxey et al. [14] and developed by Maxey & Patel [15], Lomholt et al. [16] and Lomholt & Maxey [17]. Fluid is

assumed to fill the whole flow domain, including the volume occupied by the bubbles. The presence of each bubble is represented by a finite force monopole that generates a body force distribution $\mathbf{f}(\mathbf{x},t)$ on the fluid, which transmits the resultant force of the bubbles on the flow to the fluid. The velocity field $\mathbf{u}(\mathbf{x},t)$ is incompressible and satisfies

$$\nabla \cdot \mathbf{u} = 0 \tag{1}$$

$$\rho \frac{D\mathbf{u}}{Dt} = -\nabla p + \mu \nabla^2 \mathbf{u} + \mathbf{f}(\mathbf{x},t), \tag{2}$$

where μ is the fluid viscosity and p is the pressure. The body force due to the presence of N_B bubbles is

$$\mathbf{f}(\mathbf{x},t) = \sum_{n=1}^{N_B} \mathbf{F}^{(n)} \Delta(\mathbf{x} - \mathbf{Y}^{(n)}(t)), \tag{3}$$

$\mathbf{Y}^{(n)}(t)$ is the position of the nth spherical bubble and $\mathbf{F}^{(n)}$ is the force this exerts on the fluid. The force monopole for each bubble is determined by the function $\Delta(\mathbf{x})$, which is specified as a Gaussian envelope

$$\Delta(\mathbf{x}) = (2\pi\sigma^2)^{-3/2} \exp(-\mathbf{x}^2 / 2\sigma^2) \tag{4}$$

and the length scale σ is set in terms of the bubble radius a as $a/\sigma = \sqrt{\pi}$. The velocity of each bubble $\mathbf{V}^{(n)}(t)$ is found by forming a local average of the fluid velocity over the region occupied by the bubble as

$$\mathbf{V}^{(n)}(t) = \int \mathbf{u}(\mathbf{x},t)\Delta(\mathbf{x} - \mathbf{Y}^{(n)}(t))d^3\mathbf{x}. \tag{5}$$

If m_B and m_F denote the mass of a bubble and the mass of displaced fluid, the force of the bubble acting on the fluid is

$$\mathbf{F}^{(n)} = (m_B - m_F)(\mathbf{g} - \frac{d\mathbf{V}^{(n)}}{dt}). \tag{6}$$

This force is the sum of the net external force due to buoyancy of the bubble and the excess inertia of the bubble over the corresponding volume of displaced fluid. For the present study, we exclude the effects of buoyancy and the mass of the bubble is neglected. In addition a short-range, conservative force barrier is imposed to represent collisions between bubbles and prevent overlap. A similar barrier force is imposed, normal to the wall, to represent collisions between a bubble and a rigid wall.

With this scheme the body forces induce a fluid motion equivalent to that of the bubbles. The dynamics of the bubbles and the fluid are considered as one system where fluid drag on the bubbles, added-mass effects and lift forces are internal to the system. The method does not resolve flow details near to the surface of a bubble or particle, and indeed the no-slip condition is not satisfied on surface. At distances of about half a particle radius from the surface the flow though is well represented. While there is no explicit boundary condition on the bubble surface, the condition (5) ensures that the bubble and the surrounding fluid move together.

The FCM procedures gives good results for isolated particles, particle pairs and random suspensions at void fractions of up to 20%. The results have been tested against full DNS and against experiments, for both Stokes flows and for finite Reynolds number conditions, with good agreement; see Lomholt et al. [16], Liu et al. [18]. The results too are reliable for unsteady flow conditions, matching those obtained from particle-tracking equations [19].

3. TURBULENT CHANNEL FLOW

The wall boundaries of the channel flow are located at $x_2 = \pm h$ with the half-width of the channel $h = 1$. Periodic boundary conditions are applied in the streamwise, x_1 and spanwise, x_3 directions and the flow domain size $L_1 \times 2h \times L_3$ is $2\pi \times 2 \times 2\pi$. The velocity and pressure fields are represented by a Fourier expansion in x_1 and x_3, while in the wall normal direction a spectral/hp element representation in terms of Jacobi polynomials is employed, Karniadakis & Sherwin [20]. The flow evolution is computed in terms of primitive flow variables using a high-order splitting scheme [20]. In addition, a dealiasing procedure is applied in the Fourier expansion for the nonlinear terms, based on the standard 3/2-rule.

The initial flow is a fully developed turbulent channel flow, generated from earlier simulations. The turbulent flow is characterized by the friction Reynolds number, $\mathrm{Re}_* = u_* h / \nu$ where ν is the kinematic viscosity and ρu_*^2 is the mean frictional wall shear stress. To date, we have completed series of simulations for $\mathrm{Re}_* = 135$, 200 and 400. The numerical resolution at the lowest Reynolds number is 64^3, which numerical tests showed was sufficient to resolve the flow. At the higher Reynolds numbers the mesh is $128 \times 145 \times 128$. In the simulations, the volume flow rate is held constant and the pressure gradient adjusted to maintain this. The fluid velocity is scaled so that the mean bulk velocity is 0.667.

The micro-bubbles are initially seeded in the near-wall region of a turbulent channel flow in planar layers parallel to the walls. The motion of the bubbles and the flow is computed from the system of equations (1-6). Bubbles that exit the domain in the streamwise or spanwise directions are reintroduced into the flow, matching the periodic boundary conditions for the flow. The bubble radius a/h ranges from 0.05 to 0.3. The bubble radius may also be specified in terms of wall variables as $a^+ = u_* h / \nu$.

	$\mathrm{Re}_* = 135$				$\mathrm{Re}_* = 400$				
Radius, a/h	0.075	0.1	0.15	0.3	0.05	0.05	0.05	0.075	0.1
a^+	10	13.5	20	40.5	20	20	20	30	40
N_B	2450	800	242	60	7,200	14,400	21,600	2,450	800
Average void fraction	5.5%	4.24%	4.3%	8.6%	4.8%	9.6%	15.3%	5.5%	4.24%
Seed at y^+	11	20	25	50	24	24	24	32	60
Drag Reduction, %	10	7-8	2.5	0.5	3-3.5	6	6.5	3	2.5

Table 1: Simulation parameters and estimated level of drag reduction

4. RESULTS

In this section we provide an overview of the simulation results. Table 1 gives a summary of simulation conditions used for $\mathrm{Re}_* = 135$ and 400, giving the range of bubble

sizes as *a/h* and in terms of wall variables. The initial distance of the bubbles from the wall is given as y^+, for the layer closest to the wall. Results are also reported in [9], [21].

Figure 1 shows the time variation in the drag force at Re* = 135 for different bubble sizes following the introduction of the bubbles into the flow and this is compared to the turbulent drag without bubbles. The drag force is evaluated by integrating the viscous shear stress over each wall and normalizing this by the mean drag in the absence of bubbles. The results show that the drag force decreases initially and then reaches an ambient level that may be sustained at levels of 8 to 10%, depending on bubble size. Bubbles of size $a^+ = 40$, not shown in the figure, produced very little drag reduction, except for a short initial transient as the bubbles dispersed away from the wall [9].
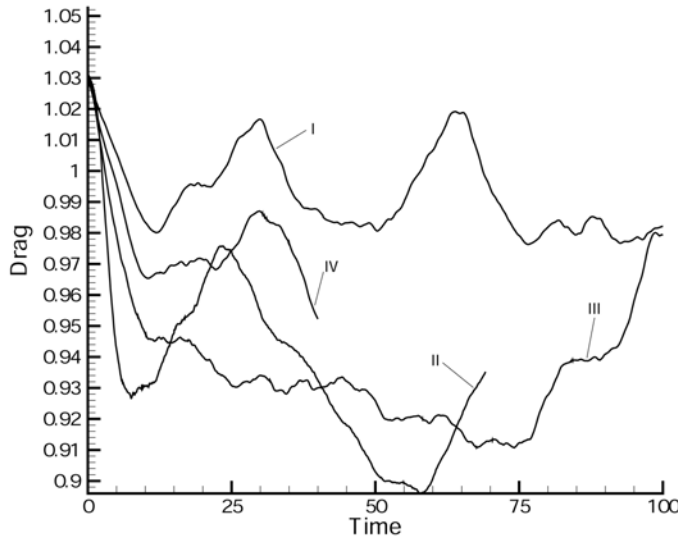
Figure 1: Normalized drag force at Re*=135: I, no bubbles; II, a+=10; III, a+=13.5; IV, a+=20.

The profile for the bubble void fraction is evaluated as

$$c(x_2,t) = \left\langle \frac{1}{\rho} \sum_{n=1}^{N_B} m_F \Delta(\mathbf{x} - \mathbf{Y}^{(n)}) \right\rangle \qquad (7)$$

where the angle brackets indicate a spatial average over the homogeneous directions x_1, x_3.
The evolution of the void fraction profile is shown in figure 2 for the bubbles with $a^+ = 10$ and in figure 3 for $a^+ = 13.5$. The bubbles disperse away from the wall, gradually becoming more uniformly distributed throughout the flow and the near-wall concentration drops. This is similar between the two different bubble sizes. The near-wall peaks reflect the initial seeding of the flow and the bubble size determines how close to the wall the bubbles can be introduced. Seeding the flow uniformly with 800 bubbles $a^+ = 13.5$ gives a similar level of drag reduction but this is not as strong and the near-wall concentration levels are lower [21].
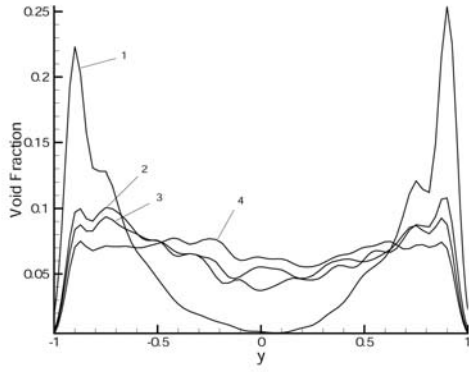
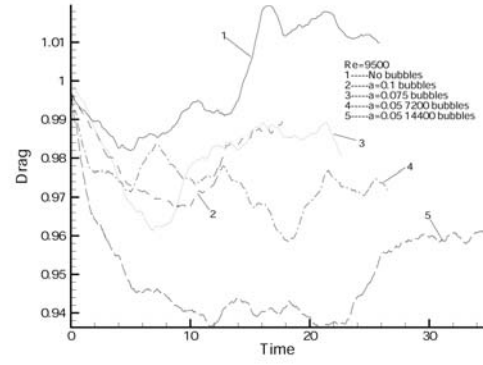**Figure 2: Bubble void fraction for a+=10: 1, t=20; 2, t=40; 3, t=60; 4, t=80.**

Figure 5: Normalized drag for Re*=400: 1, no bubbles; 2, a+=40; 3, a+=30; 4, a+=20 (5%); 5, a+=20 (10%).

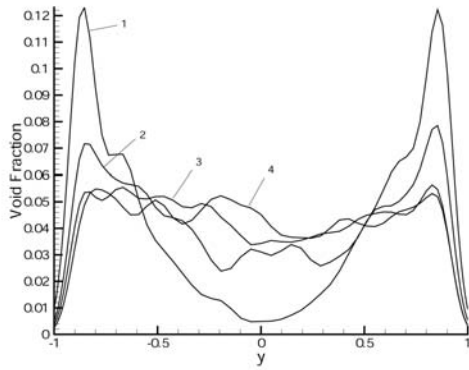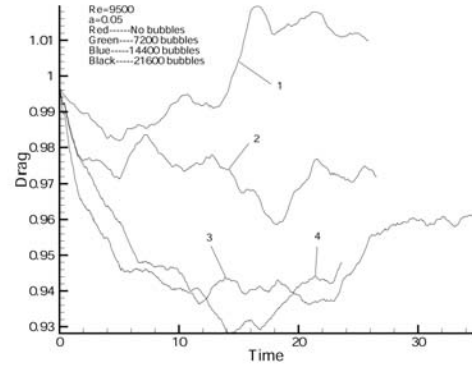**Figure 3: Bubble voiud fraction for a+=13.5: 1, t=20; 2, t=40; 3, t=60; 4, t=80.**

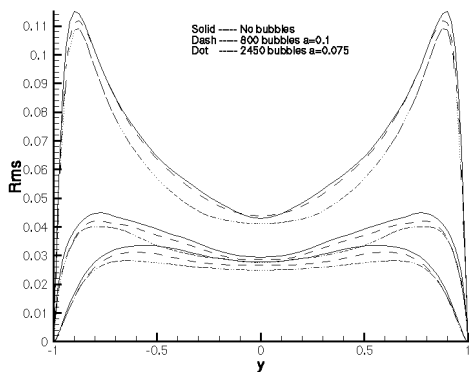**Figure 6: Normalized drag for Re*=400 and a+=20: 1, no bubbles; 2, 4.8% void; 3, 9.6% void; 4, 14.3% void.**

Figure 4: RMS fluctuations for Re*=135: _____, no bubbles; ----, a+=13.5; ....., a+=10.

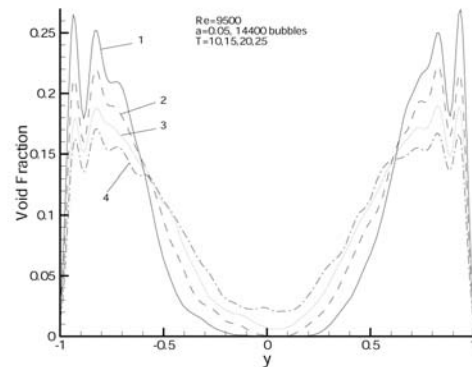**Figure 7: Void fraction profiles for Re*=400, a+=20, 14400 bubbles: 1, t=10; 2, t=15; 3, t=20; 4, t=25.**

The pressure gradient required to drive the flow adjusts in order to maintain a constant volumetric flow rate through the channel. The total flow is combination of the liquid phase flow rate Q_L and the total flow due the motion of the bubbles

$$Q_B = \frac{1}{\rho} \sum_{n=1}^{N_B} m_F V_1^{(n)} \qquad (8)$$

The sum $Q_L + Q_B$ is constant. As the bubbles disperse away from the wall into the faster moving flow they accelerate and Q_B increases. The wall drag and the pressure gradient both decrease during this initial stage [9], but this effect is less significant after the initial transient.

Figure 4 shows profiles of the rms fluctuations in the turbulent velocities for Re$_*$ = 135 and for the bubbles a^+ = 10 and 13.5. These are given as $\langle u_1^2 \rangle$ etc., directly in terms of the flow variables u_i without conditional averaging between the liquid or bubble phases, and averaged over the time interval of the simulation. The results are in dimensional units and compare the values with and without bubbles present. Clearly the smaller bubbles produce a significant reduction in all the velocity fluctuations.

We now consider results for Re$_*$ = 400. Figure 5 shows the time variation in the drag force for a range of bubble sizes with a^+ varying from 20 to 40. Limits on numerical resolution prevented us from simulating smaller bubbles. At a similar void fraction of 4-5% the bubbles of size a^+ = 20 give similar levels of drag reduction between the two Reynolds numbers. Also we see that even the larger bubbles give a measurable level of drag reduction. At higher Reynolds numbers the range of the viscous and inertial sublayers extends further in terms of wall units. The time scales of near-wall dynamics are also relatively shorter.

Seeding the flow with a larger number of bubbles also contributes to a higher level of drag reduction as shown in figure 6. Here the bubbles are all of size a^+ = 20 and additional bubbles are seeded in extra layers parallel to the walls. This is illustrated by the void fraction profiles in figure 7 where two layers adjacent to each wall were used. One effect of the extra bubbles is to counter the effects of turbulent dispersion and maintain the near-wall concentration for longer.
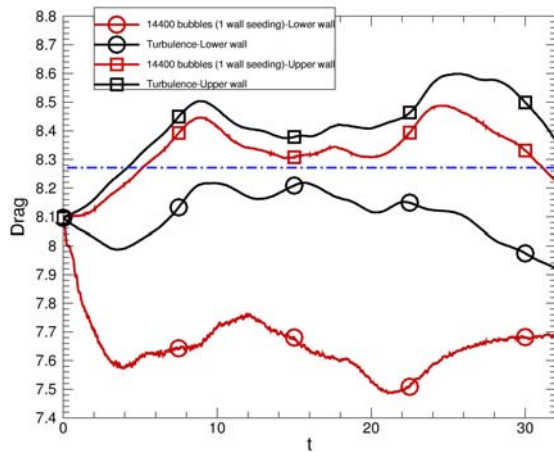

Figure 8: Drag force at Re*=200 for a+=10, one-wall seeding: black, no bubbles; red, bubbles; O, lower wall; squares, upper wall
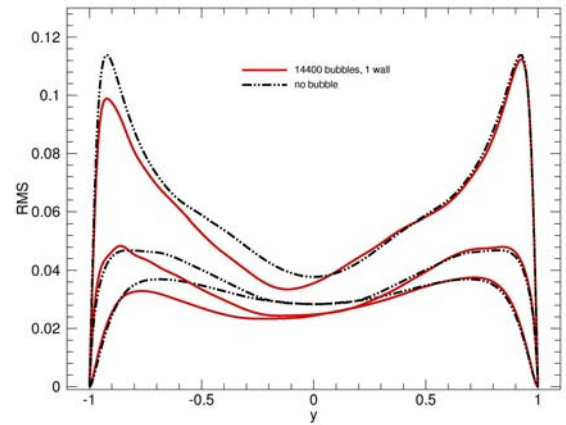

Figure 9: RMS fluctuation profiles at Re*=200, one-wall seeding: _ . ._.._ , no bubbles; _____, bubbles a+=10.

At Re$_*$ = 200 we examine the effects of seeding just one wall in the flow with bubbles. The lower wall, $x_2 = -h$, is seeded with 14,400 bubbles in multiple layers up to an average void fraction of 9.6%. The bubble radius is $a/h = 0.05$ or $a^+ = 10$. The multiple layers ensure that the near-wall concentration is maintained. At the lower wall, as shown in figure 8, the drag is reduced and is even somewhat reduced on the upper wall. The corresponding profiles of the rms velocity fluctuations are plotted in figure 9. At the upper wall there is little change in the turbulent velocity fluctuations, as compared to the flow without bubbles, while at the lower walls the turbulence levels are attenuated.

5. FLOW ANALYSIS

An equation for the combined two-phase flow may be derived from the momentum equation (2) and from (6). This becomes

$$\frac{\partial}{\partial t}(\rho u_i) - \frac{d}{dt}\left(\sum_{n=1}^{N_B} m_F V_i^{(n)} \Delta(\mathbf{x} - \mathbf{Y}^{(n)})\right) = -\nabla p + \mu \nabla^2 u_i$$

$$-\frac{\partial}{\partial x_j}\left\{\rho u_i u_j - \sum_{n=1}^{N_B} m_F V_i^{(n)} V_j^{(n)} \Delta(\mathbf{x} - \mathbf{Y}^{(n)})\right\}$$

(9)

The terms on the left-hand side of (9) correspond to the rate of change of the momentum of the bubble-liquid mixture. As the bubbles have negligible mass they carry no momentum and their contribution appears as a momentum deficit. The last group of terms on the right-hand side of (9) gives rise to a modified Reynolds stress

$$\left\langle -\rho u_i u_j + \sum_{n=1}^{N_B} m_F V_i^{(n)} V_j^{(n)} \Delta(\mathbf{x} - \mathbf{Y}^{(n)}) \right\rangle$$

(10)

From these two groups of terms we could form conditional averages for the fluid phase momentum and Reynolds stresses. In practice this is difficult to do with the present data as the flow is not stationary and the mean bubble concentration is changing continuously.

The form of the modified Reynolds stress (10) indicates that one effect of the bubbles, if they moved perfectly with the local fluid velocity, is a density effect that would reduce the effective flux of turbulent momentum transfer. This is not as significant as might appear at first. Xu et al. [21] reported on a comparison of simulations with solid particles $m_P = 2m_F$ at Re$_*$ =135 for radius $a/h = 0.05$ and an average void fraction of 4.24%. This choice for the particle mass causes an exact sign change in the force (6) transmitted by the particle to the fluid as compared to a bubble. This would also reverse the sign in the Reynolds stress term in (10). The particles produce a modest increase in drag of about 3% while the drag reduction by the bubbles is close to 8%. This indicates that the correlation between the bubble motion and the turbulence is more significant than the density effect alone.

6. SUMMARY

From the results presented here, and other simulation results we have obtained, certain observations may be made.

- The near-wall concentration of the bubbles is an important factor and when this drops to a low level the drag reduction effect is diminished or eliminated. This indicates that the interactions of the bubbles with the near-wall turbulence are critical.
- Smaller bubbles in general are more effective in reducing drag. Wall variable scales for the bubble radius provide a fair correlation of the results, as is illustrated by the results for $a^+ = 20$ between the two Reynolds numbers in table 1.
- At higher Reynolds numbers the range of bubble sizes a^+ that may be effective in reducing drag appears to be broader.
- The main effect of increasing the bubble seeding levels at higher Reynolds numbers is to screen the bubbles closest to the wall and inhibit the loss by dispersion.

REFERENCES

1. M.E. McCormick and R. Bhattacharyya, 1973. Drag reduction of a submersible hull by electrolysis. Nav. Eng. J. **85**, 11.
2. N.K. Madavan, S. Deutsch and C.L. Merkle, 1984. Reduction of turbulent skin friction by microbubbles. Phys. Fluids **27**, 356-363.
3. N.K. Madavan, S. Deutsch and C.L. Merkle, 1985. Measurements of local skin friction in a microbubble-modified turbulent boundary layer. J. Fluid Mech. **156**, 237-256.
4. C.L. Merkle and S. Deutsch, 1989. Microbubble drag reduction. *Frontiers in Experimental Fluid Mechanics, Lecture Notes in Engineering*, edited by M. Gad-el-Hak, Springer-Verlag, vol. 46, 291.
5. H. Kato, M. Miyanaga, H. Yamaguchi and M.M. Guin, 1995. Frictional drag reduction by injecting bubbly water into turbulent boundary layer and the effect of plate orientation. *Advances in Multiphase Flow*, edited by A. Serizawa, T. Fukano and J. Bataille, Elsevier Science. Proc. 2nd Intl. Conf. Multiphase Flow, Kyoto, Japan, 85-96.
6. M.M. Guin, H. Kato and Y. Takahashi, 1998. Experimental evidence for a link between microbubble drag reduction phenomena and periodically excited wall-bounded turbulent flow. In *Proceedings of the International Symposium on Seawater Drag Reduction*, Newport RI, 22-23 July 1998, 313-318.
7. H. Kato, T. Iwashina, M. Miyanaga and H. Yamaguchi, 1999. Effects of microbubbles on the structure of turbulence in a turbulent boundary layer. J. Mar. Sci. Technol. **4**, 155-162.
8. Proceedings of the Symposium on Smart Control of Tubulence, http://www.turbulence-control.gr.jp/sympo_e/
9. J. Xu, M.R. Maxey and G.E. Karniadakis, 2002. Numerical simulation of turbulent drag reduction using micro-bubbles. J. Fluid Mech. **468**, 271-281.
10. Kanai & H. Miyata, 2001. Direct numerical simulation of wall turbulent flows with microbubbles. Int. J. Numer. Meth. Fluids **35**, 593-615.
11. T. Kawamura & Y. Kodama, 2002. Numerical simulation method to resolve interactions between bubbles and turbulence. Intl. J. Heat & Fluid Flow **23**, 627-638.
12. J. Magnaudet and I. Eames, 2000. The motion of high Reynolds number bubbles in inhomogeneous flows. Ann. Rev. Fluid Mech. **32**, 659-708.
13. R. Detsch, 1991. Small air bubbles in reagent grade water and seawater: I. Rise velocities of 20 to 1000 μm diameter bubbles. J. Geophys. Res. **96**, 8901-8906.

14. M.R. Maxey, B.K. Patel, E.J. Chang and L-P. Wang, 1997. Simulations of dispersed turbulent multiphase flow. Fluid Dynamics Research **20**, 143-156.
15. M.R. Maxey and B.K. Patel, 2001. Localized force representations for particles sedimenting in Stokes flow. Int. J. Multiphase Flow **27**, 1603-1626.
16. S. Lomholt, B. Stenum and M.R. Maxey, 2002. Experimental verification of the force-coupling method for particulate flows. Int. J. Multiphase Flow **28**, 225-246.
17. S. Lomholt and M.R. Maxey, 2003. Force-coupling method for particles sedimenting in a channel: Stokes flow. J. Comp. Phys., in press.
18. D. Liu, M.R. Maxey and G.E. Karniadakis, 2002. A fast method for particulate microflows. J. Microelectromechanical Systems, to appear.
19. M.R. Maxey and J.J. Riley, 1983. Equation of motion for a small rigid sphere in a non-uniform flow. Phys. Fluids. **26**, 883-889.
20. G.E. Karniadakis and S.J. Sherwin, 1999. *Spectral/hp Element Methods for CFD.* Oxford University Press.
21. J. Xu, M.R. Maxey and G.E. Karniadakis, 2003. DNS of turbulent drag reduction using microbubbles. AIAA paper 2003-1280, 41st Aerospace Science Meeting, Reno, Nevada.